

# **Lawrence Berkeley National Laboratory**

## **LBL Publications**

### **Title**

Promising thermoelectric performance in van der Waals layered SnSe<sub>2</sub>

### **Permalink**

<https://escholarship.org/uc/item/1jc2c7hc>

### **Authors**

Wu, Yixuan

Li, Wen

Faghaninia, Alireza  
et al.

### **Publication Date**

2017-12-01

### **DOI**

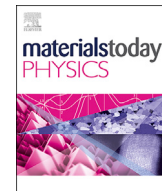
10.1016/j.mtphys.2017.10.001

Peer reviewed



Contents lists available at ScienceDirect

## Materials Today Physics

journal homepage: <https://www.journals.elsevier.com/materials-today-physics>Promising thermoelectric performance in van der Waals layered SnSe<sub>2</sub>Yixuan Wu <sup>a</sup>, Wen Li <sup>a</sup>, Alireza Faghaninia <sup>b</sup>, Zhiwei Chen <sup>a</sup>, Juan Li <sup>a</sup>, Xinyue Zhang <sup>a</sup>, Bo Gao <sup>a</sup>, Siqi Lin <sup>a</sup>, Binqiang Zhou <sup>a</sup>, Anubhav Jain <sup>b</sup>, Yanzhong Pei <sup>a,\*</sup><sup>a</sup> Interdisciplinary Materials Research Center, School of Materials Science and Engineering, Tongji Univ., 4800 Caoan Rd., Shanghai 201804, China<sup>b</sup> Energy Storage and Distributed Resources Division, Lawrence Berkeley National Laboratory, Berkeley, CA 94720, USA

## ARTICLE INFO

## Article history:

Received 25 September 2017

Received in revised form

30 September 2017

Accepted 2 October 2017

Available online xxxx

## ABSTRACT

SnSe as a lead-free IV–VI semiconductor, has attracted intensive attention for its potential thermoelectric applications, since it is less toxic and much cheaper than conventional PbTe and PbSe thermoelectrics. Here we focus on its sister layered compound SnSe<sub>2</sub> in n-type showing a thermoelectric performance to be similarly promising as SnSe in the polycrystalline form. This is enabled by its favorable electronic structure according to first principle calculations, its capability to be effectively doped by bromine on selenium site to optimize the carrier concentration, as well as its intrinsic lattice thermal conductivity as low as 0.4 W/m·K due to the weak van der Waals force between layers. The broad carrier concentration ranging from 0.5 to  $6 \times 10^{19}$  cm<sup>-3</sup> realized in this work, further leads to a fundamental understanding on the material parameters determining the thermoelectric transport properties, based on a single parabolic band (SPB) model with acoustic scattering. The layered crystal structure leads to a texture in hot-pressed polycrystalline materials and therefore anisotropic transport properties, which can be well understood by the SPB model. This work not only demonstrates SnSe<sub>2</sub> as a promising thermoelectric material but also guides the further improvements particularly by band engineering and texturing approaches.

© 2017 Elsevier Ltd. All rights reserved.

## 1. Introduction

Based on either Seebeck or Peltier effect, thermoelectrics enable a direct conversion between heat and electricity, showing a great impact on both power generation and refrigeration [1,2]. The performance of a thermoelectric material device primarily depends on the materials dimensionless thermoelectric figure of merit,  $zT = S^2T/\rho(\kappa_E + \kappa_L)$ , where  $S$ ,  $\rho$ ,  $\kappa_E$ ,  $\kappa_L$  and  $T$  are the Seebeck coefficient, electrical resistivity, electronic thermal conductivity, lattice thermal conductivity and absolute temperature, respectively. As can be seen, a high thermoelectric performance requires a large Seebeck coefficient, a low electrical resistivity and a low thermal conductivity. However,  $S$ ,  $\rho$  and  $\kappa_E$ , are strongly coupled with each other, a simple improvement in one of these three parameters usually results in a compensation in the other two, leading to the difficulty for improving  $zT$  [3,4].

Electronically, since these three parameters are strongly related to the band structure, band engineering approaches are demonstrated to decouple these parameters for an enhancement in power

factor  $S^2/\rho$  [5–7]. Successful strategies are typified by a large band degeneracy through band convergence [8] and band nestification [9,10], as well as a low inertial mass [11]. These approaches are demonstrated to be effective, particularly in IV–VI thermoelectrics such as PbTe [12,13], PbSe [14], SnTe [15] and GeTe [16] with a high band degeneracy. Importantly, these strategies guarantee a high  $zT$  only when the carrier concentration is optimized [17–20]. This is due to the fact that a maximization on both power factor ( $S^2/\rho$ ) and  $zT$  requires a certain position of Fermi level [21], corresponding to a narrow range of carrier concentration. Such an optimal carrier concentration is found to depend strongly on the temperature and the density of states effective mass [22]. Therefore, maximizing the thermoelectric performance fundamentally requires an effective carrier concentration optimization through doping.

Thermally, a minimization in lattice thermal conductivity ( $\kappa_L$ ), the only one independent material parameter determining  $zT$ , has also been proven to be effective for enhancing  $zT$ . Successful strategies are typified by alloying [23], dislocations [24,25] and nano-structuring [26–28] as effective scattering sources of phonons for minimizing the mean free path due to strong phonon scattering. This has been demonstrated in many IV–VI thermoelectrics including PbTe [29], PbSe [30], SnTe [31] and GeTe [32]. Alternatively, intrinsic low lattice thermal conductivity due to a strong

\* Corresponding author.

E-mail address: [yanzhong@tongji.edu.cn](mailto:yanzhong@tongji.edu.cn) (Y. Pei).

lattice anharmonicity [33], existence of liquid-like ions [34], a low sound velocity [35] as well as crystal structure complexity [3] has been proven to be effective for achieving a high thermoelectric performance in many materials as well [36–40].

Utilization of the above mentioned strategies has led to a great advancement in IV–VI thermoelectrics [41–44], yet, the toxicity of Pb and scarcity of Te and Ge can be a big concern for large-scale and eco-friendly applications. This motivates much effort to the design and realization of non-toxic and low-cost thermoelectrics. Among these materials, SnSe is found to be particularly interesting due to its intrinsically strong lattice anharmonicity [45] causing a low lattice thermal conductivity and its multiple band degeneracy all of which lead to a high figure of merit particularly in single crystals [46,47].

SnSe<sub>2</sub> is another semiconducting member of IV–VI showing a composition as eco-friendly as SnSe; it might show promising thermoelectric performance as well. This compound crystallizes in a layered structure, as usually found in metal dichalcogenides MCh<sub>2</sub> (M = Sn, Ti, Zr, Hf and Ch = S, Se, Te) [48]. Its semiconducting characteristics is predicted theoretically and confirmed experimentally [49]. It shows interesting optoelectronic and electrochemical properties, which attracts much attention for potential applications as lithium ion batteries [50], field effect transistors [51,52], photovoltaic [53] and infrared devices [54]. Its potential as high performance thermoelectrics stems from: 1) its layered structure where the existence of weak chemical bonds produces a low sound velocity for an intrinsic low lattice thermal conductivity; and 2) a wide enough band gap (~1 eV) [55,56] as well as a high band degeneracy in the vicinity of both conduction and valence bands. Such features are believed to be largely responsible for the high thermoelectric performance observed in both newly developed SnSe [46] as well as conventional Bi<sub>2</sub>Te<sub>3</sub> thermoelectrics [57].

Existing study on thermoelectric SnSe<sub>2</sub> mostly focus on first principles calculations, and a promising *zT* of ~0.9 is predicted in bulk material particularly in n-type conduction [58]. Furthermore, theoretical calculations on the formation energy of various doping defects suggest donors are more stable than acceptors [59]. Experimentally, Ag-doping on the cation sited does not enable a p-type conduction and the resulting n-type materials show a very low carrier concentration and thus a low *zT* of only ~0.3 [60]. This indicates the necessity of an effective doping for a high carrier concentration to fully realize the high thermoelectric performance, especially in n-type conduction.

This motivates the current experimental work focusing on n-type polycrystalline SnSe<sub>2</sub>, with a broad range of carrier concentration ( $0.5\text{--}6 \times 10^{19}\text{ cm}^{-3}$ ), which is enabled by Br-doping. This not only helps understand the fundamental electronic transport properties, but also realizes a promising *zT* of 0.6 with the help of an intrinsic lattice thermal conduction as low as 0.4 W/m-K (at ~750 K) resulting from the weak chemical bonds. Such a low  $\kappa_L$  is largely attributable to the very large inter-layer distance (~3.1 Å) for a weak van der Waals bond and thus a very low cross-layer sound velocity (as shown in Fig. 1), and the longitudinal branch usually contributes largely to the lattice thermal conductivity due to its high group velocity [61,62]. This can be understood from the propagation of a sound wave in solid, liquid and gas and lower sound velocity in presence of weaker chemical bonds. Furthermore, the strong anisotropy in crystal structure results in an anisotropic band structure and enables a texture to be obtained even in hot pressed materials; the directional transport properties can be well understood based on a single parabolic band model with acoustic scattering. Band structure calculations reveal the existence of multiple valley degeneracy in the conduction bands, suggesting possible enhancement in thermoelectric performance when these bands are engineered to converge. This work demonstrates SnSe<sub>2</sub> as a

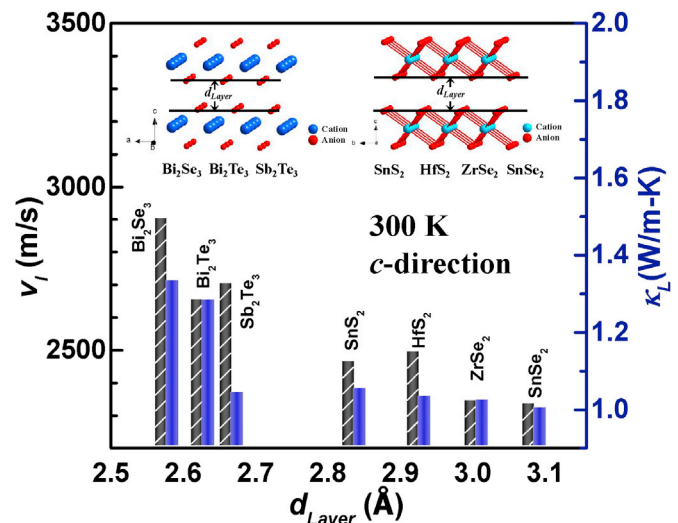


**Fig. 1.** Inter-layer distance ( $d_{Layer}$ ) dependent cross-layer longitudinal sound velocity and lattice thermal conductivity at room temperature for Bi<sub>2</sub>Te<sub>3</sub>-type thermoelectrics [58,65–69] and metal dichalcogenides (MCh<sub>2</sub>) [70–72] with similar layered crystal structures.

promising thermoelectric material; the achieved *zT* in SnSe<sub>2</sub> is very comparable to that of polycrystalline SnSe with carrier concentration tuning only [63,64].

## 2. Materials and methods

Polycrystalline SnSe<sub>2</sub> samples with doping were synthesized by a melting, quenching and hot pressing technique. Dopants including Nb, Cu, Br were used to tune the carrier concentration and Br is found to be the most effective. The stoichiometric amount of high purity elements (Sn>99.99%, Se>99.99%) and compound (SnBr>98%) were melted at 1023 K for 6 h, followed by quenching in cold water and annealing at 850 K for 3 days. The obtained ingots were ground for hot pressing by induction heating at 800 K for 30 mins under a uniaxial pressure of ~60 MPa.

The phase composition of the samples were identified by powder X-ray diffraction (XRD, DX2700) and scanning electron microscope (SEM, Phenom Pro) equipped with energy dispersive spectrometer (EDS). The thermal diffusivity ( $\lambda$ ) was measured by a laser flash technique (Netzsch LFA457). The thermal conductivity ( $\kappa$ ) was calculated by the equation  $\kappa = d\lambda C_p$ ; where  $C_p$  is the specific heat capacity obtained from literature [73] and  $d$  is the density estimated by a mass/volume method. The electrical transport properties including Seebeck coefficient ( $S$ ), Hall coefficient ( $R_H$ ), and resistivity ( $\rho = 1/\sigma$ ) of the pellet samples were measured simultaneously from 300 to 750 K, during both heating and cooling. The Seebeck coefficient was obtained from the slope of the voltage vs. temperature gradients of 0–5 K; the resistivity and Hall coefficient were measured using van der Pauw technique with a reversible magnetic field of 1.5 T. The measurement uncertainty for  $S$ ,  $\rho$  and  $\kappa$  is 5% approximately.

Sound velocities (longitudinal and transverse branches) were measured on the hot-pressed samples at room temperature by using pulse-receiver (Olympus-NDT) equipped with an oscilloscope (Keysight). Optical reflectance was measured by a Fourier Transform Infrared Spectroscopy (FTIR, Bruker Tensor 2 equipped with a diffuse reflectance attachment) at room temperature.

Density functional theory (DFT) calculations were performed using the Vienna ab initio simulation package (VASP) [74]. We used the Perdew-Burke-Enzerhof (PBE) generalized gradient approx-

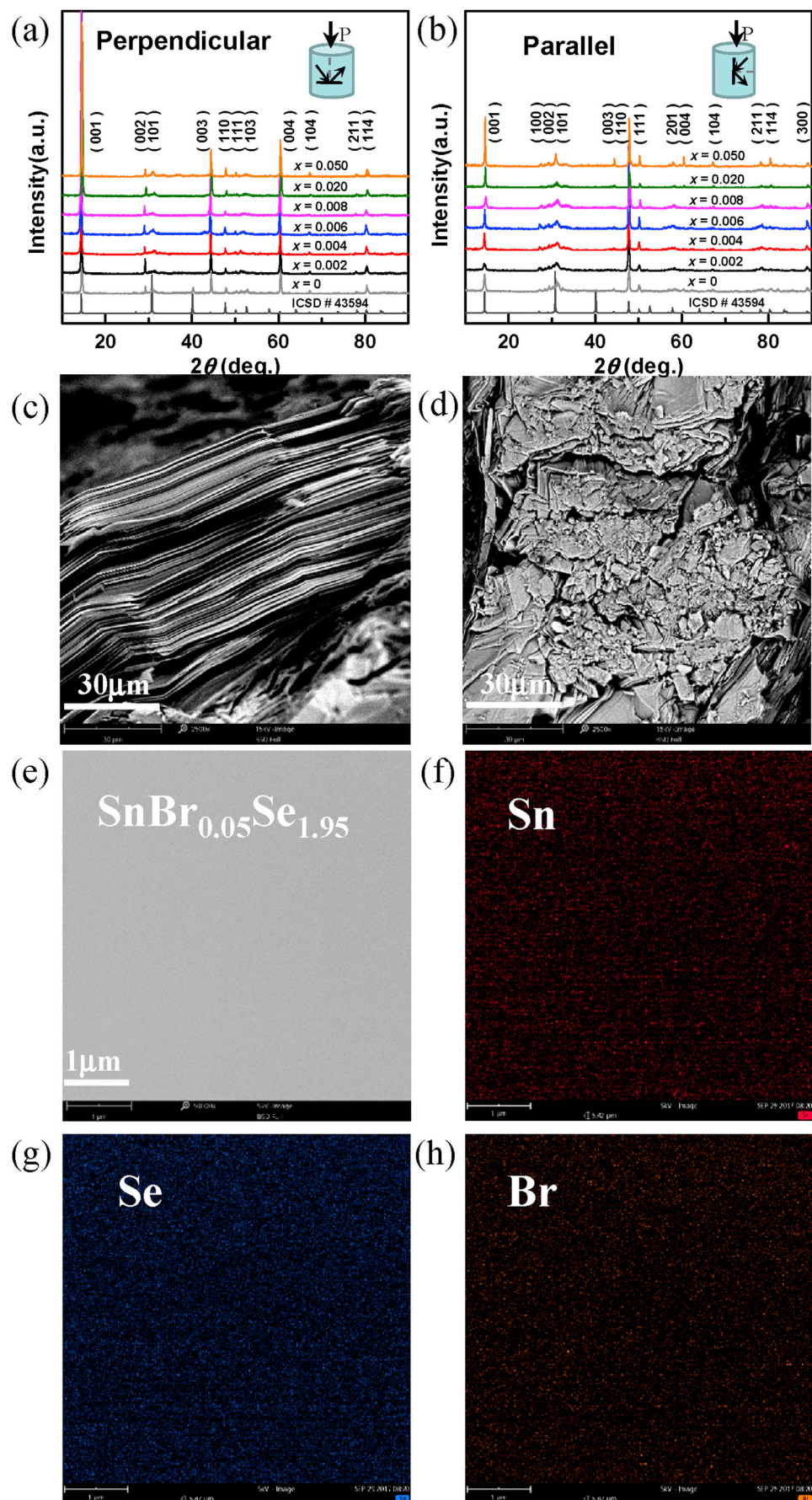


**Fig. 2.** The XRD patterns of pellet samples along directions Perpendicular (a) and Parallel (b) to that of hot pressing. SEM images of fracture surfaces along Parallel (c) and Perpendicular (d) directions for  $\text{SnBr}_{0.05}\text{Se}_{1.95}$ . SEM images of a cleavage surface with the corresponding mapping on compositions by EDS for  $\text{SnBr}_{0.05}\text{Se}_{1.95}$  (e–h).

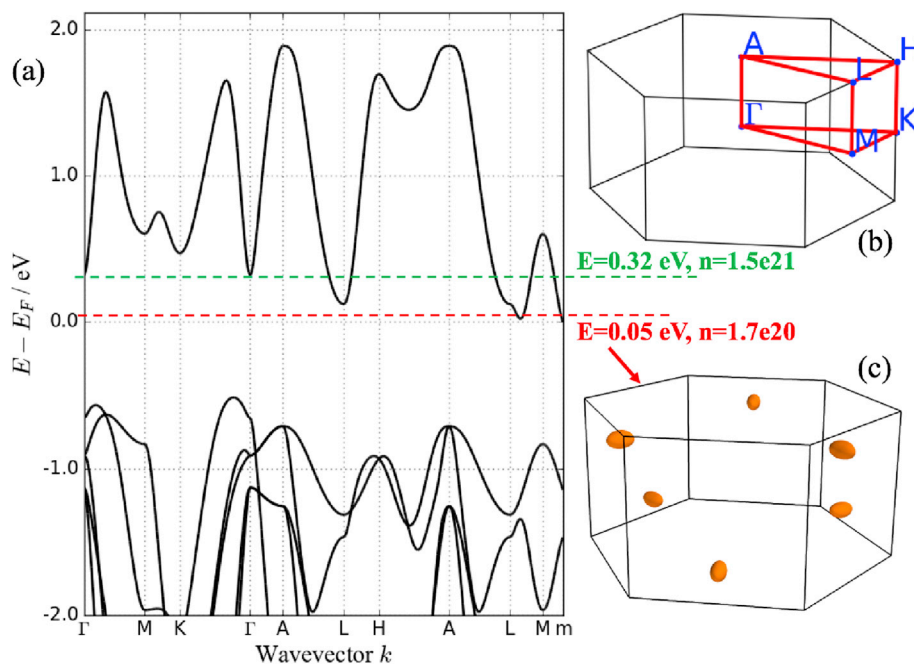


**Fig. 3.** Calculated band structure and correspondence of Fermi energy versus carrier concentration at room temperature (a), Brillouin zone with high-symmetry points (b), and the Fermi surface at 0.05 eV below the conduction band edge (c) for SnSe<sub>2</sub>.

imation (GGA) [75] exchange-correlation functional and the projected augmented-wave (PAW) [76,77] method to model core electrons. The band structure and elastic properties calculations were performed using atomate workflow management package

[78]. To include the van der Waals interaction in layered SnSe<sub>2</sub>, we employed DFT-D2 [79] functional as implemented in VASP. The calculated lattice parameters agree well with the experiment (See Table S1). The full  $6 \times 6$  elastic tensor, shear and bulk moduli and

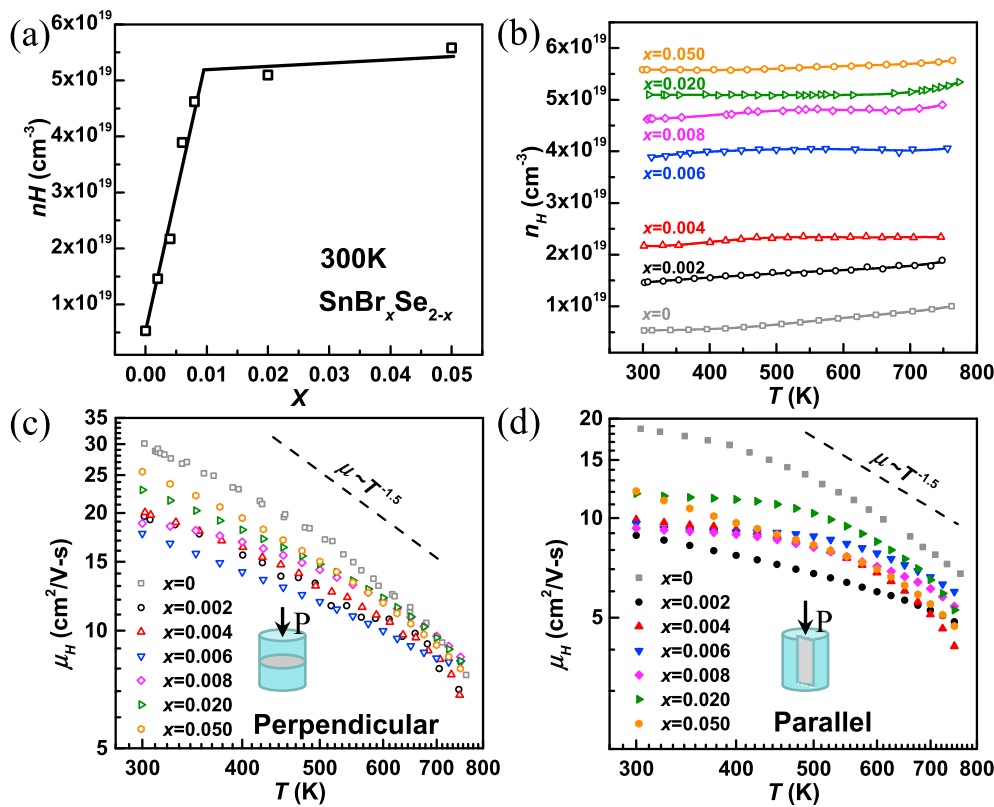


**Fig. 4.** Composition dependent Hall carrier concentration at room temperature (a), and temperature dependent Hall carrier concentration (b) Hall mobility (c for Perpendicular and d for Parallel) for SnBr<sub>x</sub>Se<sub>2-x</sub>.

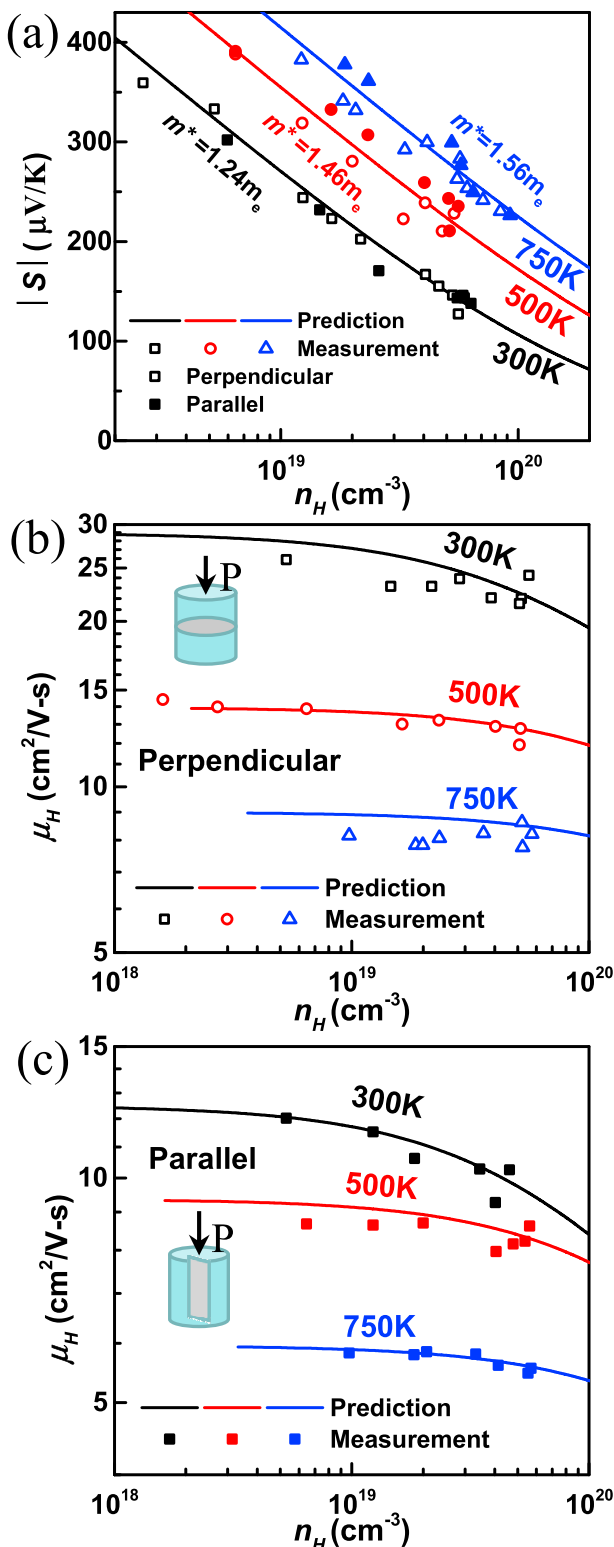


**Fig. 5.** (a) Hall carrier concentration dependent Seebeck coefficient and Hall mobility ( $\mu_H$ ) along Perpendicular (b) and Parallel (c) directions.

longitudinal and transverse sound velocities were calculated by applying various deformations to fit the elastic tensor using Green-Lagrange strain tensor. Further details on the elastic calculation methodology is available elsewhere [80,81]. For a more rigorous structural and electronic convergence as well as consistency

between the band structure and elastic calculations we chose a high energy cutoff of 700 eV and set total energy convergence criteria to  $10^{-6}$  eV. To calculate the average effective mass, we employed the method described by Hautier et al. [82] and using the BoltzTraP code [83]. It should be noted that the effective mass values are independent of the relaxation time constant in BoltzTraP formulation and are provided as a function of the Fermi level (i.e., of temperature and carrier concentration). We also used BoltzTraP to calculate the carrier concentration at different energy levels in the conduction bands based on the density of state (DOS) and Fermi-Dirac distribution.

### 3. Results and discussion

$\text{SnSe}_2$  crystallizes in a rhombohedral structure with layers of Sn atom plane sandwiched by two Se atom planes [84] (Fig. 1). The large distance between layers ( $\sim 3.1 \text{ \AA}$ ) indicates a van der Waals bond feature [85]. The X-ray diffraction results for  $\text{SnBr}_x\text{Se}_{2-x}$  pellets sliced along directions perpendicular (marked as ‘Perpendicular’, Fig. 2a) and parallel (marked as ‘Parallel’, Fig. 2b) to that of pressure applied during hot pressing. All the diffraction peaks match well with the layered rhombohedral structure (ICSD#43594). It can be seen that the relative intensities of  $(00l)$  diffraction peaks are much stronger in Perpendicular pellets than those in Parallel ones. The integral intensities of  $(00l)$  diffraction peaks enable an estimation of orientation factor ( $F$ ) of 0.78 for Perpendicular pellets and of 0.22 for Parallel ones, respectively, according to the Lotgering method [86]. This indicates the layered crystal structure drives the hot-pressed polycrystalline materials to be textured, as can be further evidenced from the SEM images on fracture surfaces for  $\text{SnBr}_{0.05}\text{Se}_{1.95}$  (Fig. 2c–d). SEM images of a cleavage surface and corresponding compositional mapping by EDS for  $\text{SnBr}_{0.05}\text{Se}_{1.95}$  further confirm the phase purity and homogeneity of the material obtained here (Fig. 2e–h).

The DFT-D2 calculated band structure and the corresponding Fermi surface of the conduction band of  $\text{SnSe}_2$  are shown in Fig. 3. The comparison of  $\text{SnSe}_2$  band structure in absence and in presence of van der Waals (VdW) interactions calculated in VASP with GGA functional is shown in Fig. S1. The band structure reveals an indirect band gap of 0.59 eV; the conduction band minimum (CBM) is located slightly inside the Brillouin zone (BZ), close to the L–M path on the face of the BZ. The k-point at which the CBM is located has the fractional coordinates of (0.47, 0.00, -0.30) and is denoted by  $m$  in Fig. 3a. This creates a band degeneracy of 6 as shown in Fig. 3c. The density of states effective mass near the conduction band edge is  $m_{\text{DOS}}^* = 1.16 m_e$ . The conduction band minimum is found to be anisotropic as indicated by a heavier band mass along the c direction ( $m_{b,c}^* = 0.41 m_e$ ) than that along ab plane ( $m_{b,ab}^* = 0.32 m_e$ ), leading to an expectation of a higher mobility along ab plane. The second lowest valley in the conduction band is located at the zone center ( $\Gamma$  point), 0.32 eV above the conduction band minimum. When the Fermi level is at this edge, the corresponding carrier concentration is about  $1.5 \times 10^{21} \text{ cm}^{-3}$  at room temperature, indicating single band transport behavior at lower carrier concentrations. It is interesting to note that the large band degeneracy and the possibility of involving the second band indicate further potential to optimize n-type  $\text{SnSe}_2$  for thermoelectric applications.

Doping with Br at Se site successfully enables an increase of room temperature Hall carrier concentration ( $n_H$ ) from 0.5 to  $5.6 \times 10^{19} \text{ cm}^{-3}$  (Fig. 4a) with a saturation at  $x \sim 0.01$ . The nearly temperature independent Hall carrier concentration (Fig. 4b) indicates the overall degenerated conduction by a single band in majority of the samples obtained in this work. This is consistent with the band structure calculations (Fig. 3) since the experimental carrier concentration falls in a range of conduction by a single band.

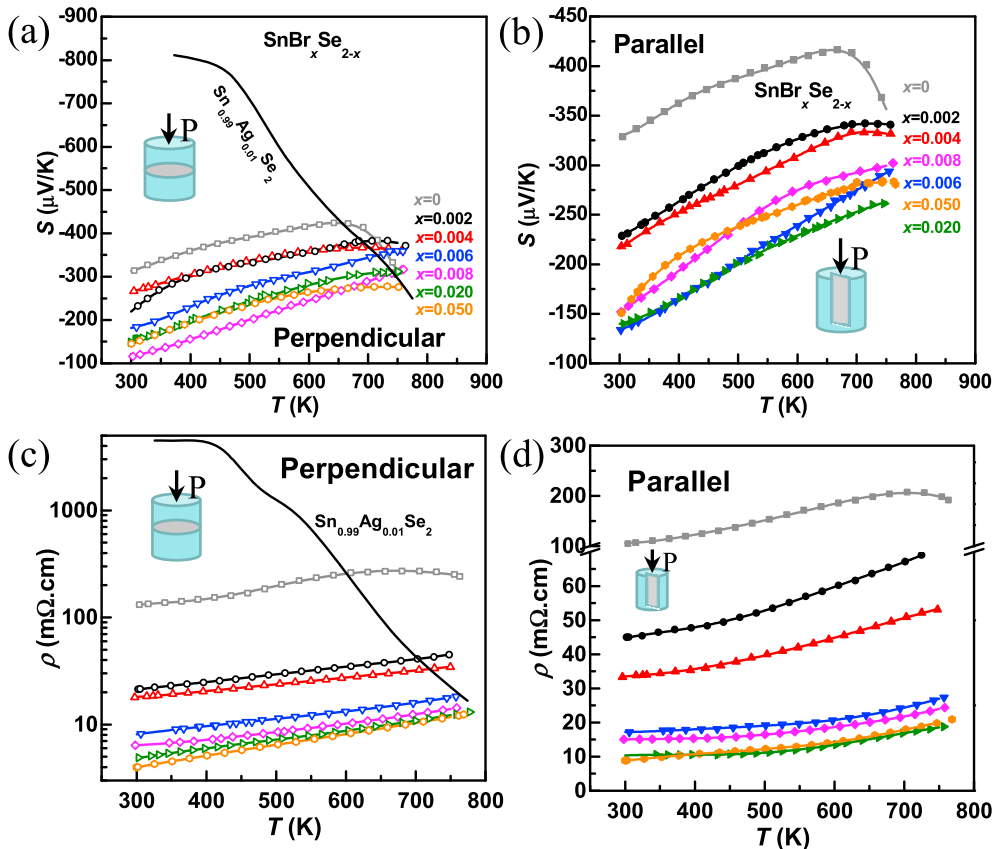


**Fig. 6.** Temperature dependent Seebeck coefficient (a, b), resistivity (c, d) along Perpendicular (a, c) and Parallel (b, d) directions for  $\text{SnBr}_x\text{Se}_{2-x}$ , with a comparison to those of  $\text{Sn}_{0.99}\text{Ag}_{0.01}\text{Se}_2$  [60].

The Hall mobility ( $\mu_H$ ) for all the samples decreases with increasing temperature via  $T^{-1.5}$ , indicating a dominant scattering mechanism of charge carriers by acoustic phonons in the whole temperature range (Fig. 4c and d). From the XRD results in Fig. 2, it is seen that  $\text{SnSe}_2$  doped with 5% Br has the best crystallinity among all the samples, which might explain the higher Hall mobility observed in this sample (Fig. 4). It should also be noted that the determination of Hall mobility could involve accumulative uncertainties from the resistivity and Hall measurements.

The broad range of carrier concentration enabled by Br-doping leads to a fundamental understanding on the transport properties

of  $\text{SeSe}_2$  according to the single parabolic band (SPB) model. Both the measured Hall carrier concentration dependent Seebeck coefficient and Hall mobility agree well with the model predictions at different temperatures in a broad carrier concentration range ( $10^{18}$ – $10^{20} \text{ cm}^{-3}$ ), as shown in Fig. 5. It should be noted that the Hall mobility along Perpendicular direction is higher than that along Parallel direction, which is consistent with the calculated anisotropy in the effective mass (Table S2). While the carrier concentration dependent Seebeck coefficient show no observable difference.

Similar direction and carrier concentration dependent transport properties can be found as well at high temperatures as shown in

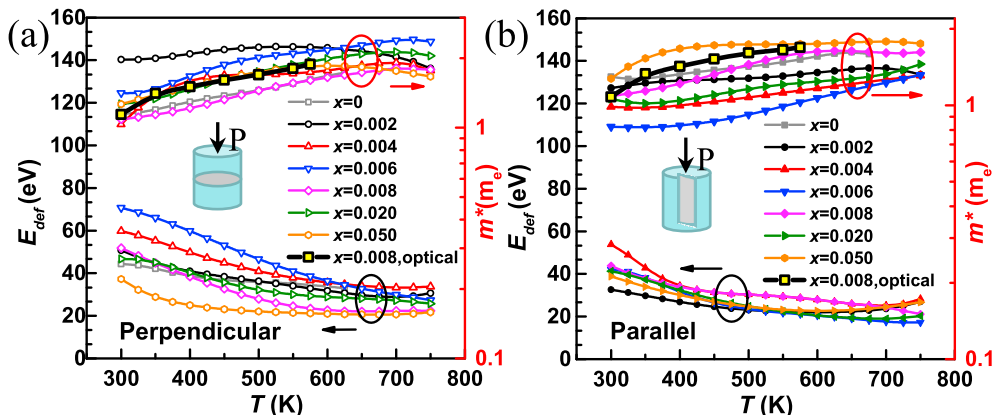


**Fig. 7.** Temperature dependent deformation potential coefficient ( $E_{\text{def}}$ ) and Density of states effective mass ( $m^*$ ) for both Perpendicular (a) and Parallel (b) directions for  $\text{SnBr}_x\text{Se}_{2-x}$ . The density of states effective mass estimated by optical measurements for  $\text{Sn}_{0.008}\text{Se}_{1.992}$  is also included for comparison.

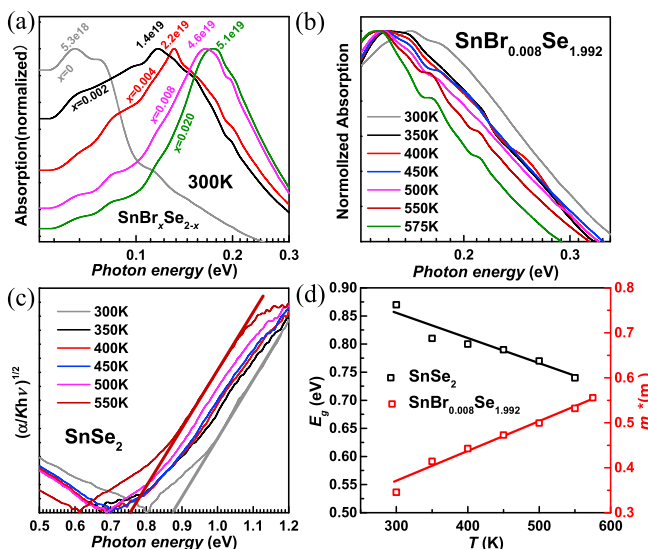


**Fig. 8.** Composition dependent infrared absorption for  $\text{SnBr}_x\text{Se}_{2-x}$  at room temperature (a), temperature dependent absorption by free carriers for  $\text{SnBr}_{0.008}\text{Se}_{1.992}$  (b) and absorption between band edges for  $\text{SnSe}_2$  (c). The resultant temperature dependent optical band gap and inertial mass are given in (d).

**Fig. 6.** Comparing with Ag-doped  $\text{SnSe}_2$  [60], the current work achieves a much lower Seebeck coefficient compared to Ag-doped [60] due to the much higher carrier concentration. For the majority of the samples, Seebeck coefficients and resistivities increase with increasing temperature, showing a degenerated semiconducting behavior. Negative Seebeck coefficients indicates an n-type

conduction for all the samples. Similar Seebeck coefficients are observed along different directions. While the resistivity is much lower along the Perpendicular direction than that along Parallel one, which is due to the anisotropic band structure/Hall mobility as discussed above. The samples, including the high- $zT$  ones, are measured under a couple of thermal cycles during both heating and cooling. The consistent transport properties in high- $zT$  samples indicate the stability of the materials in the temperature range measured (Fig. S2). However, pristine  $\text{SnSe}_2$  shows a low carrier concentration and a hysteresis in transport properties, indicating a dominant mechanism of native defects (probably Se vacancies) controlling the carrier concentration.

The temperature dependent transport properties further enables the estimations of both the Density of states effective mass ( $m^*$ ) and the deformation potential coefficient ( $E_{\text{def}}$ ) according to the SPB model, with the knowledge of a band degeneracy ( $N_V$ ) of 6 from the band structure calculations (Fig. 3). It is seen from Fig. 7 that  $m^*$  slightly increases from  $\sim 1.24 \text{ m}_e$  at 300 K to  $\sim 1.56 \text{ m}_e$  at 750 K, which is presumably related to the lattice expansion. Such a temperature dependence on  $m^*$  is frequently observed in IV–VI semiconductors [11]. The room temperature Density of states effective mass ( $m^* \sim 1.24 \text{ m}_e$ ) from this method agrees well with the band calculations ( $m^* \sim 1.16 \text{ m}_e$ , Fig. 3). The deformation potential coefficient ( $E_{\text{def}}$ ), measuring the strength of carrier scattering by acoustic phonons, is found to be overall temperature independent at  $T > \sim 550 \text{ K}$ . While at lower temperatures, the carrier mobility is lower than that under a pure acoustic scattering mechanism (Fig. 4c and d), leading to an overestimation of  $E_{\text{def}}$  at these temperatures. The obtained  $E_{\text{def}} \sim 25 \text{ eV}$  (at  $T > \sim 550 \text{ K}$ ) is very comparable with that of PbTe [22].

To further understand the transport properties, optical absorption measurements are carried out. The photon energy of the

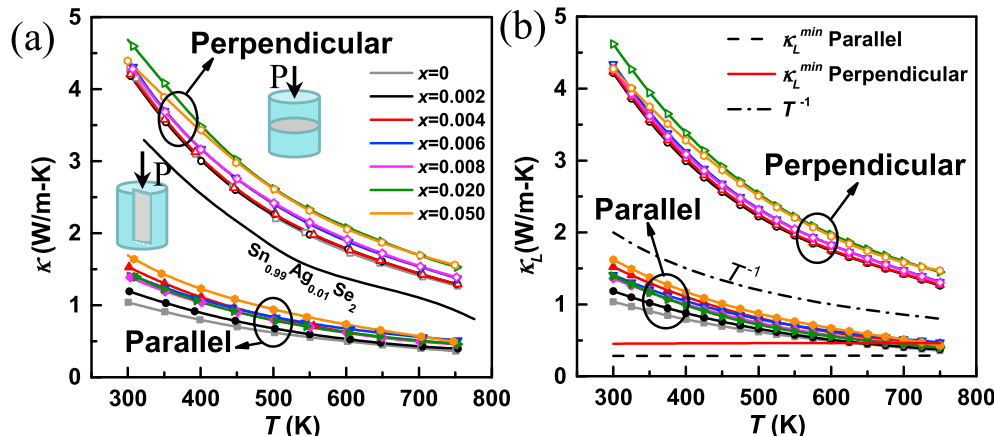


**Fig. 9.** Temperature dependent thermal conductivity (a) and lattice thermal conductivity (b) along Perpendicular and Parallel directions for  $\text{SnBr}_x\text{Se}_{2-x}$ , with a comparison to those of  $\text{Sn}_{0.99}\text{Ag}_{0.01}\text{Se}_2$  [60].

**Table 1**

Elastic properties from measurements and DFT calculations for  $\text{SnSe}_2$  at room temperature.

Elastic properties	Perpendicular	Parallel	DFT-D2 calculations
Longitudinal sound velocity (m/s)	3430 Measurement	2260 Measurement	2350
Transverse sound velocity (m/s)	1950 Measurement	1120 Measurement	1520
Mean velocity (m/s)	2170	1250	
$\kappa_L^{\min}$ (W/m-K)	0.46	0.28	0.34
$\theta_D$ (K)	218.7	126.4	
Gruneisen parameter	1.55	2.04	
Poisson's ratio	0.26	0.34	
Bulk modulus (GPa)	39.61	20.60	14.47
Shear modulus (GPa)	22.67	7.42	13.80

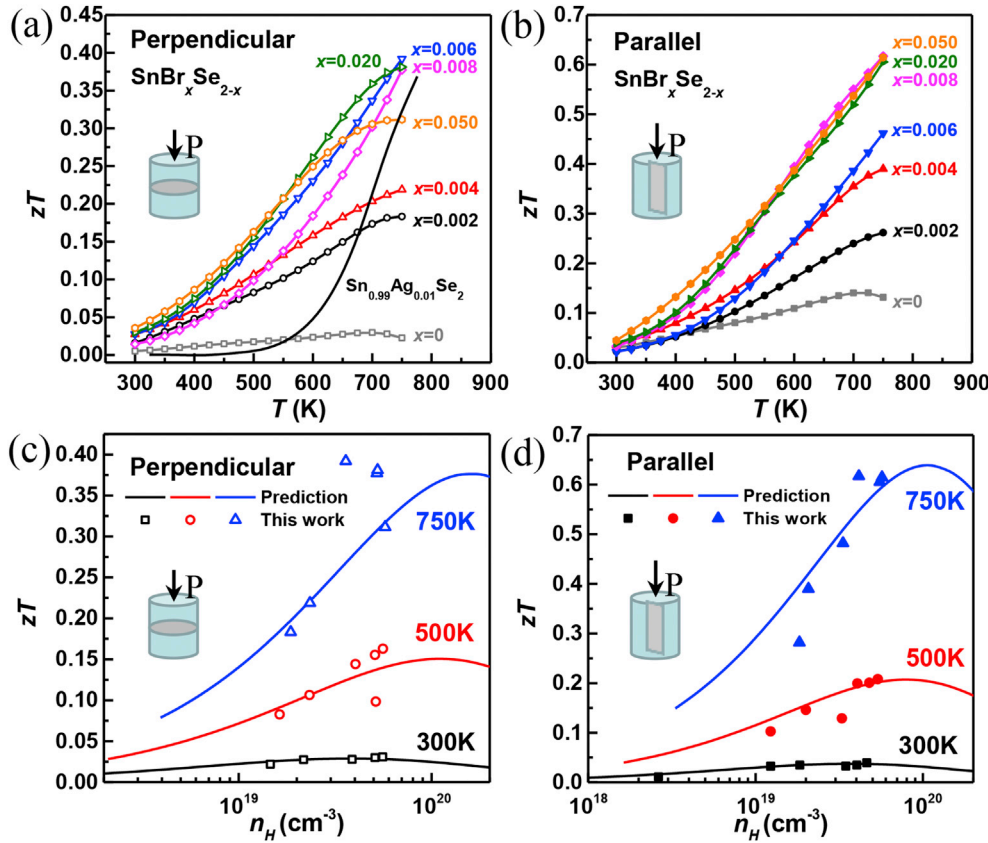


**Fig. 10.** Thermoelectric figure of merit ( $zT$ ) (a, b) by measurement and by model prediction (c, d) along both Perpendicular (a, c) and Parallel (b, d) directions for  $\text{SnBr}_x\text{Se}_{2-x}$ .

absorption peak due to carriers is found to increase with increasing doping level (Fig. 8a). Utilization of Lyden method [87] enables an estimation of inertial mass from this measurement, with the measured carrier concentration and mobility as well as the dielectric constant [70]. The estimated inertial mass ( $m_l^*$ ) is about  $0.35 m_e$  for all doping levels, indicating a rigid band behavior in the carrier concentration range obtained in this work. Same measurement at high temperature for  $\text{SnBr}_{0.008}\text{Se}_{1.992}$  (Fig. 8b) reveals an increase in  $m_l^*$  with increasing temperature (Fig. 8d). Under an isotropic band approximation (the band mass  $m_b^*$  and inertial mass  $m_l^*$  are indetical), the estimated density of state mass ( $m^* = m_b^* N_V^{2/3}$ ) agree well with that obtained by SPB model in a wide temperature range (Fig. 7). Absorption between band edges enables an estimation of the indirect band gap to be  $\sim 0.9$  eV at room temperature (Fig. 8c), which is consistent with the literature results ( $\sim 1$  eV) [55]. Moreover, the band gap is found to decrease with temperature (Fig. 8c). Such a wide energy gap ensures a weak effect on the transport properties due to thermally excited minority carriers (Fig. 6).

Due to the weak van der Waals force between the layers of  $\text{SnSe}_2$  (Fig. 1), the lattice thermal conductivity ( $\kappa_L$ ) is expected to be low due to the low sound velocity as shown in Fig. 9. Further due to the layered structure, the resultant texture in these polycrystalline materials show anisotropic thermal conductivities. The  $\kappa_L$  is obtained by subtracting the electronic thermal conductivity ( $\kappa_E = LT/\rho$ ) from the total thermal conductivity, where  $L$  is the Lorenz factor determined by the single parabolic band (SPB) model with acoustic scattering.  $\kappa_L$  decreases with increasing temperature with a rough  $T^{-1}$  relationship, indicating a dominant phonon scattering by Umklapp process in these materials. The  $\kappa_L$  along Perpendicular direction is found to be as low as  $\sim 0.4$  W/m-K at  $T > 600$  K,

approaching the armorous limit according to the Cahill model [88]. Measurement of sound velocity offers a clue to the origin of such a low  $\kappa_L$ . The elastic properties are list in Table 1. Comparing to the mean sound velocity ( $v_s = 1620$  m/s [89]) of conventional  $\text{Bi}_2\text{Te}_3$  with a similar layered structure,  $\text{SnSe}_2$  is found to have an even smaller  $v_s$  of  $\sim 1250$  m/s along Parallel direction, although the average atomic mass is much lighter. This indicates an even weaker van der Waals force produces low frequency phonon modes for a low  $\kappa_L$  in  $\text{SnSe}_2$ . With a more detailed comparison among similar layered compounds as shown in Fig. 1, it is seen that larger interlayer distance leads to weaker bonds and therefore slower longitudinal sound velocity and lower lattice thermal conductivity. It should be noted that such a sound velocity observed in  $\text{SnSe}_2$  is one of the lowest in known semiconductors [35] with potential thermoelectric applications. The elastic properties by DFT calculations agree with the measurements (Table 1 and S1). Through a full elastic tensor calculation, the minimal lattice thermal conductivity is estimated to be 0.34 W/m-K, according to the Cahill-Pohl minimum thermal conductivity model. It should be noted that doping would introduce point defects for scattering phonons and then possibly result in a reduction in lattice thermal conductivity ( $\kappa_L$ ). However, the mass and size contrasts between Se and Br are sufficiently small, therefore, a strong point defect scattering is not expected here. The difference in  $\kappa_L$  observed in Fig. 9 is presumably due to the different degree of texture (Fig. 2) from sample to sample in this strong isotropic material. In addition, the determination of  $\kappa_L$  could also involve multiple uncertainties due to the estimation of Lorenz factor ( $L$ ) and the measurements of resistivity ( $\rho$ ) and total thermal conductivity to cause the difference observed.

With the help of intrinsically low lattice thermal conductivity in this layered structure material, the measured thermoelectric figure

of merit (peak  $zT$ -0.6) (Fig. 10) is found to be as promising as SnSe by only tuning the carrier concentration. Using the average  $k_L$ , effective mass ( $m^*$ ) and deformation potential coefficient ( $E_{def}$ ), the SPB model further enables a prediction on carrier concentration dependent  $zT$  at different temperatures, which reasonably agrees with the measurements along both Perpendicular and Parallel directions.

#### 4. Summary

Weak van der Waals force due to large distance between layers of  $\text{SnSe}_2$  leads to an extremely low sound velocity and thus an intrinsic lattice thermal conduction approaching its armorphous limit. Doping with Br at Se site enables a broad carrier concentration for understanding the transport properties, which can be well described by a single parabolic band model. These features lead to a figure of merit as promising as that in SnSe via only carrier concentration optimization. Band calculations reveal the existence of highly degenerated conduction band and possibility of involving additional bands for further enhancements through convergence of conduction bands. The layered structure also leads to texture dependent transport properties, indicating the importance of texturing for further improvement in  $zT$ . This work demonstrates  $\text{SnSe}_2$  as an eco-friendly and promising thermoelectric material.

#### Acknowledgement

This work is supported by the National Natural Science Foundation of China (Grant No. 51422208, 11474219 and 51772215) and the national Recruitment Program of Global Youth Experts (1000 Plan). A Faghaninia and A Jain acknowledge the computational resources support from the National Energy Research Supercomputing Center (NERSC), a DOE Office of Science User Facility supported by the Office of Science of the U.S. Department of Energy.

#### Appendix A. Supplementary data

Supplementary data related to this article can be found at <https://doi.org/10.1016/j.mtphys.2017.10.001>.

#### References

- [1] L.E. Bell, Cooling, heating, generating power, and recovering waste heat with thermoelectric systems, *Science* 321 (2008) 1457–1461.
- [2] F.J. Disalvo, Thermoelectric cooling and power generation, *Science* 285 (1999) 703–706.
- [3] G.J. Snyder, E.S. Toberer, Complex thermoelectric materials, *Nat. Mater.* 7 (2008) 105–114.
- [4] W. Liu, J. Hu, S. Zhang, M. Deng, C.-G. Han, Y. Liu, New trends, strategies and opportunities in thermoelectric materials: a perspective, *Mater. Today Phys.* 1 (2017) 50–60.
- [5] Y. Pei, H. Wang, G.J. Snyder, Band engineering of thermoelectric materials, *Adv. Mater.* 24 (2012) 6125–6135.
- [6] H. Xie, H. Wang, Y. Pei, C. Fu, X. Liu, G.J. Snyder, X. Zhao, T. Zhu, Beneficial contribution of alloy disorder to electron and phonon transport in half-heusler thermoelectric materials, *Adv. Funct. Mater.* 23 (2013) 5123–5130.
- [7] J. Mao, Y. Wu, S. Song, J. Shuai, Z. Liu, Y. Pei, Z. Ren, Anomalous electrical conductivity of n-type Te-doped  $\text{Mg}_3\text{Sb}_1.5\text{Bi}_{0.5}$ , *Mater. Today Phys.* 3 (2017) 1–6.
- [8] Y. Pei, X. Shi, A. Lalonde, H. Wang, L. Chen, G.J. Snyder, Convergence of electronic bands for high performance bulk thermoelectrics, *Nature* 473 (2011) 66–69.
- [9] Q. Zhang, F. Cao, K. Lukas, W. Liu, K. Esfarjani, C. Opeil, D. Broido, D. Parker, D.J. Singh, G. Chen, Z. Ren, Study of the thermoelectric properties of lead selenide doped with boron, gallium, indium, or thallium, *J. Am. Chem. Soc.* 134 (2012) 17731–17738.
- [10] S. Lin, W. Li, Z. Chen, J. Shen, B. Ge, Y. Pei, Tellurium as a high-performance elemental thermoelectric, *Nat. Commun.* 7 (2016) 10287.
- [11] Y. Pei, A.D. Lalonde, H. Wang, G.J. Snyder, Low effective mass leading to high thermoelectric performance, *Energy Environ. Sci.* 5 (2012) 7963–7969.
- [12] J. Koenig, M. Nielsen, Y.-B. Gao, M. Winkler, A. Jacquot, Titanium forms a resonant level in the conduction band of PbTe, *Phys. Rev. B* 84 (2011), 205126.
- [13] Z. Jian, Z. Chen, W. Li, J. Yang, W. Zhang, Y. Pei, Significant band engineering effect of YbTe for high performance thermoelectric PbTe, *J. Mater. Chem. C* 3 (2015) 12410–12417.
- [14] Q. Zhang, F. Cao, W. Liu, K. Lukas, B. Yu, S. Chen, C. Opeil, D. Broido, G. Chen, Z. Ren, Heavy doping and band engineering by potassium to improve the thermoelectric figure of merit in p-type PbTe, PbSe, and  $\text{PbTe}_{(1-y)}\text{Se}_{(y)}$ , *J. Am. Chem. Soc.* 134 (2012) 10031–10038.
- [15] W. Li, Z. Chen, S. Lin, Y. Chang, B. Ge, Y. Chen, Y. Pei, Band and scattering tuning for high performance thermoelectric  $\text{Sn}_{1-x}\text{Mn}_x\text{Te}$  alloys, *J. Mater. Chem. C* 3 (2015) 307–315.
- [16] J. Li, Z. Chen, X. Zhang, Y. Sun, J. Yang, Y. Pei, Electronic origin of the high thermoelectric performance of GeTe among the p-type group IV monotellurides, *NPG Asia Mater.* 9 (2017) e353.
- [17] Q. Zhang, E.K. Chere, K. Mcenaney, M. Yao, F. Cao, Y. Ni, S. Chen, C. Opeil, G. Chen, Z. Ren, Enhancement of thermoelectric performance of n-type PbSe by Cr doping with optimized carrier concentration, *Adv. Energy Mater.* 5 (2015), 1401977.
- [18] W. Li, Y. Wu, S. Lin, Z. Chen, J. Li, X. Zhang, L. Zheng, Y. Pei, Advances in environment-friendly SnTe thermoelectrics, *ACS Energy Lett.* 2 (2017) 2349–2355.
- [19] T. Zhu, Y. Liu, C. Fu, J.P. Heremans, J.G. Snyder, X. Zhao, Compromise and synergy in high-efficiency thermoelectric materials, *Adv. Mater.* 29 (2017), 1605884.
- [20] Q. Zhang, H. Wang, W. Liu, H. Wang, B. Yu, Q. Zhang, Z. Tian, G. Ni, S. Lee, K. Esfarjani, G. Chen, Z. Ren, Enhancement of thermoelectric figure-of-merit by resonant states of aluminum doping in lead selenide, *Energy Environ. Sci.* 5 (2012) 5246–5251.
- [21] H.J. Goldsmid, *Introduction to Thermoelectricity*, vol. 121, Springer, 2010.
- [22] Y. Pei, Z.M. Gibbs, A. Gloskovskii, B. Balke, W.G. Zeier, G.J. Snyder, Optimum carrier concentration in n-type PbTe thermoelectrics, *Adv. Energy Mater.* 4 (2014), 1400486.
- [23] Y. Xu, W. Li, C. Wang, J. Li, Z. Chen, S. Lin, Y. Chen, Y. Pei, Performance optimization and single parabolic band behavior of thermoelectric MnTe, *J. Mater. Chem. A* 5 (2017) 19143–19150.
- [24] S.I. Kim, K.H. Lee, H.A. Mun, H.S. Kim, S.W. Hwang, J.W. Roh, D.J. Yang, W.H. Shin, X.S. Li, Y.H. Lee, G.J. Snyder, S.W. Kim, Thermoelectrics. Dense dislocation arrays embedded in grain boundaries for high-performance bulk thermoelectrics, *Science* 348 (2015) 109–114.
- [25] J. Xin, H. Wu, X. Liu, T. Zhu, G. Yu, X. Zhao, Mg vacancy and dislocation strains as strong phonon scatterers in  $\text{Mg}_2\text{Si}_{1-x}\text{Sb}_x$  thermoelectric materials, *Nano Energy* 34 (2017) 428–436.
- [26] Y. Pei, J. Lensch-Falk, E.S. Toberer, D.L. Medlin, G.J. Snyder, High thermoelectric performance in PbTe due to large nanoscale  $\text{Ag}_2\text{Te}$  precipitates and La doping, *Adv. Funct. Mater.* 21 (2011) 241–249.
- [27] A. Minnich, M. Dresselhaus, Z. Ren, G. Chen, Bulk nanostructured thermoelectric materials: current research and future prospects, *Energy Environ. Sci.* 2 (2009) 466–479.
- [28] L. Zhao, S. Hao, S. Lo, C.I. Wu, X. Zhou, Y. Lee, H. Li, K. Biswas, T.P. Hogan, C. Uher, C. Wolverton, V.P. Dravid, M.G. Kanatzidis, High thermoelectric performance via hierarchical compositionally alloyed nanostructures, *J. Am. Chem. Soc.* 135 (2013) 7364–7370.
- [29] Z. Chen, Z. Jian, W. Li, Y. Chang, B. Ge, R. Hanus, J. Yang, Y. Chen, M. Huang, G.J. Snyder, Y. Pei, Lattice dislocations enhancing thermoelectric PbTe in addition to band convergence, *Adv. Mater.* 29 (2017), 1606768.
- [30] Z. Chen, B. Ge, W. Li, S. Lin, J. Shen, Y. Chang, R. Hanus, G.J. Snyder, Y. Pei, Vacancy-induced dislocations within grains for high-performance PbSe thermoelectrics, *Nat. Commun.* 8 (2017) 13828.
- [31] Y. Pei, L. Zheng, W. Li, S. Lin, Z. Chen, Y. Wang, X. Xu, H. Yu, Y. Chen, B. Ge, Interstitial point defect scattering contributing to high thermoelectric performance in SnTe, *Adv. Electron. Mater.* 2 (2016), 1600019.
- [32] J. Li, X. Zhang, S. Lin, Z. Chen, Y. Pei, Realizing the high thermoelectric performance of GeTe by Sb-doping and Se-alloying, *Chem. Mater.* 29 (2016) 605–611.
- [33] D.T. Morelli, V. Jovovic, J.P. Heremans, Intrinsically minimal thermal conductivity in cubic I-VI-VI semiconductors, *Phys. Rev. Lett.* 101 (2008), 035901.
- [34] H. Liu, X. Shi, F. Xu, L. Zhang, W. Zhang, L. Chen, Q. Li, C. Uher, T. Day, G.J. Snyder, Copper ion liquid-like thermoelectrics, *Nat. Mater.* 11 (2012) 422–425.
- [35] W. Li, S. Lin, B. Ge, J. Yang, W. Zhang, Y. Pei, Low sound velocity contributing to the high thermoelectric performance of  $\text{Ag}_3\text{SnSe}_6$ , *Adv. Sci.* 3 (2016), 1600196.
- [36] J. Mao, Y. Wu, S. Song, Q. Zhu, J. Shuai, Z. Liu, Y. Pei, Z. Ren, Defect engineering for realizing high thermoelectric performance in n-type  $\text{Mg}_3\text{Sb}_2$ -Based materials, *ACS Energy Lett.* (2017) 2245–2250.
- [37] J. Shen, X. Zhang, Z. Chen, S. Lin, J. Li, W. Li, S. Li, Y. Chen, Y. Pei, Substitutional defects enhancing thermoelectric CuGaTe<sub>2</sub>, *J. Mater. Chem. A* 5 (2017) 5314–5320.
- [38] J. Shuai, J. Mao, S. Song, Q. Zhang, G. Chen, Z. Ren, Recent progress and future challenges on thermoelectric Zintl materials, *Mater. Today Phys.* 1 (2017) 74–95.
- [39] W.L. Siqui Lin, Shasha Li, Xinyue Zhang, Zhiwei Chen, Yidong Xu, Yue Chen, Yanzhong Pei, High thermoelectric performance of  $\text{Ag}_3\text{GaSe}_6$  enabled by low cut-off frequency of acoustic phonons, *Joule* 1 (2017) 1–15.
- [40] J. Mao, J. Shuai, S. Song, Y. Wu, R. Dally, J. Zhou, Z. Liu, J. Sun, Q. Zhang, C. Dela Cruz, S. Wilson, Y. Pei, D.J. Singh, G. Chen, C.W. Chu, Z. Ren, Manipulation of ionized impurity scattering for achieving high thermoelectric performance in

- n-type Mg<sub>3</sub>Sb<sub>2</sub>-based materials, Proc. Natl. Acad. Sci. (2017), 1711725114.
- [41] G. Tan, F. Shi, S. Hao, L.-D. Zhao, H. Chi, X. Zhang, C. Uher, C. Wolverton, V.P. Dravid, M.G. Kanatzidis, Non-equilibrium processing leads to record high thermoelectric figure of merit in PbTe–SrTe, Nat. Commun. 7 (2016) 12167.
- [42] L. Zheng, W. Li, S. Lin, J. Li, Z. Chen, Y. Pei, Interstitial defects improving thermoelectric SnTe in addition to band convergence, ACS Energy Lett. (2017) 563–568.
- [43] T. Fu, X. Yue, H. Wu, C. Fu, T. Zhu, X. Liu, L. Hu, P. Ying, J. He, X. Zhao, Enhanced thermoelectric performance of PbTe bulk materials with figure of merit  $zT > 2$  by multi-functional alloying, J. Materiom 2 (2016) 141–149.
- [44] W. Li, L. Zheng, B. Ge, S. Lin, X. Zhang, Z. Chen, Y. Chang, Y. Pei, Promoting SnTe as an eco-friendly solution for p-PbTe thermoelectric via band convergence and interstitial defects, Adv. Mater. 29 (2017).
- [45] L. Zhao, S. Lo, Y. Zhang, H. Sun, G. Tan, C. Uher, C. Wolverton, V.P. Dravid, M.G. Kanatzidis, Ultralow thermal conductivity and high thermoelectric figure of merit in SnSe crystals, Nature 508 (2014) 373–377.
- [46] L. Zhao, G. Tan, S. Hao, J. He, Y. Pei, H. Chi, H. Wang, S. Gong, H. Xu, V.P. Dravid, Ultrahigh power factor and thermoelectric performance in hole-doped single-crystal SnSe, Science (2015), aad3749.
- [47] K. Peng, X. Lu, H. Zhan, S. Hui, X. Tang, G. Wang, J. Dai, C. Uher, G. Wang, X. Zhou, Broad temperature plateau for high ZT s in heavily doped p-type SnSe single crystals, Energy Environ. Sci. 9 (2016) 454–460.
- [48] J. Robertson, Electronic structure of SnS<sub>2</sub>, SnSe<sub>2</sub>, CdI<sub>2</sub>, PbI<sub>2</sub>, Solid State Phys. 48 (1979) 4753–4766.
- [49] D.G. Mead, J.C. Irwin, Raman spectra of SnS<sub>2</sub> and SnSe<sub>2</sub>, Solid State Commun. (1976) 885–887.
- [50] C. Ling, Y. Huang, H. Liu, S. Wang, Z. Fang, L. Ning, Mechanical properties, electronic structures, and potential applications in lithium ion batteries: a first-principles study toward SnSe<sub>2</sub> Nanotubes, J. Phys. Chem. C 118 (2014) 28291–28298.
- [51] T.S. Pan, D. De, J. Manongdo, A.M. Guloy, V.G. Hadjiev, Y. Lin, H.B. Peng, Field effect transistors with layered two-dimensional SnS<sub>2-x</sub>Se<sub>x</sub> conduction channels: effects of selenium substitution, Appl. Phys. Lett. 103 (2013), 093108.
- [52] Y. Su, M.A. Ebrish, E.J. Olson, S.J. Koester, SnSe<sub>2</sub> field-effect transistors with high drive current, Appl. Phys. Lett. 103 (2013), 263104.
- [53] X. Zhou, L. Gan, W. Tian, Q. Zhang, S. Jin, H. Li, Y. Bando, D. Golberg, T. Zhai, Ultrathin SnSe<sub>2</sub> flakes grown by chemical vapor deposition for high-performance photodetectors, Adv. Mater. 27 (2015) 8035–8041.
- [54] Z. Fang, S. Hao, L. Long, H. Fang, T. Qiang, Y. Song, The enhanced photoelectrochemical response of SnSe<sub>2</sub> nanosheets, Crystengcomm 16 (2014) 2404.
- [55] M.Y. Au-Yang, M.L. Cohen, Electronic structure and optical properties of SnS<sub>2</sub> and SnSe<sub>2</sub>, Phys. Rev. 178 (1969) 1279–1283.
- [56] C.Y. Fong, M.L. Cohen, Electronic energy-band structure of SnS<sub>2</sub> and SnSe<sub>2</sub>, Phys. Rev. B 5 (1972) 3095–3101.
- [57] H. Kim, N.A. Heinz, Z.M. Gibbs, Y. Tang, S.D. Kang, G.J. Snyder, High thermoelectric performance in (Bi<sub>0.25</sub>Sb<sub>0.75</sub>)<sub>2</sub>Te<sub>3</sub> due to band convergence and improved by carrier concentration control, Mater. Today (2017) 905.
- [58] B.Z. Sun, Z. Ma, C. He, K. Wu, Anisotropic thermoelectric properties of layered compounds in SnX<sub>2</sub> (X = S, Se): a promising thermoelectric material, Phys. Chem. Chem. Phys. 17 (2015) 29844–29853.
- [59] Y. Huang, D. Zhou, X. Chen, H. Liu, C. Wang, S. Wang, First-principles study on doping of SnSe<sub>2</sub> monolayers, Chem. Phys. Chem. 17 (2016) 375–379.
- [60] F. Li, Z. Zheng, Y. Li, W. Wang, J. Li, B. Li, A. Zhong, J. Luo, P. Fan, Ag-doped SnSe<sub>2</sub> as a promising mid-temperature thermoelectric material, J. Mater. Sci. 52 (2017) 10506–10516.
- [61] G.A. Slack, The thermal conductivity of nonmetallic crystals, Solid State Phys. 34 (1979) 1–71.
- [62] P.G. Klemens, Thermal conductivity and lattice vibrational modes 7 (1958) 1–98.
- [63] C. Chen, H. Wang, Y. Chen, T. Day, G.J. Snyder, Thermoelectric properties of p-type polycrystalline SnSe doped with Ag, J. Mater. Chem. A 2 (2014) 11171–11176.
- [64] E.K. Chere, Q. Zhang, K. Dahal, F. Cao, J. Mao, Z. Ren, Studies on thermoelectric figure of merit of Na-doped p-type polycrystalline SnSe, J. Mater. Chem. A 4 (2016) 1848–1854.
- [65] Y.D. Glinka, S. Babakiray, T.A. Johnson, M.B. Holcomb, D. Lederman, Acoustic phonon dynamics in thin-films of the topological insulator Bi<sub>2</sub>Se<sub>3</sub>, J. Appl. Phys. 117 (2015), 165703.
- [66] X. Qiu, L.N. Austin, P.A. Muscarella, J.S. Dyck, C. Burda, Nanostructured Bi<sub>2</sub>Se<sub>3</sub> films and their thermoelectric transport properties, Angew. Chem. Int. Ed. 45 (2006) 5656–5659.
- [67] B. Qiu, X. Ruan, Molecular dynamics simulations of lattice thermal conductivity of bismuth telluride using two-body interatomic potentials, Phys. Rev. B 80 (2009).
- [68] R. Venkatasubramanian, Lattice thermal conductivity reduction and phonon localizationlike behavior in superlattice structures, Phys. Rev. B 61 (1999) 3091–3097.
- [69] Q. Lu, H. Zhang, Y. Cheng, X. Chen, G.-F. Ji, Phase transition, elastic and electronic properties of topological insulator Sb<sub>2</sub>Te<sub>3</sub> under pressure: first principle study, Chin. Phys. B 25 (2016), 026401.
- [70] H. Wang, Y. Gao, G. Liu, Anisotropic phonon transport and lattice thermal conductivities in tin dichalcogenides SnS<sub>2</sub> and SnSe<sub>2</sub>, Rsc. Adv. 7 (2017) 8098–8105.
- [71] D.P. Spitzer, Lattice thermal conductivity of semiconductors:a chemical bond approach, J. Phys. Chem. Solids 31 (1969) 19–40.
- [72] Q. Zhao, Y. Guo, K. Si, Z. Ren, J. Bai, X. Xu, Elastic, electronic, and dielectric properties of bulk and monolayer ZrS<sub>2</sub>, ZrSe<sub>2</sub>, HfS<sub>2</sub>, HfSe<sub>2</sub> from van der Waals density-functional theory, Phys. status solidi (b) (2017), 1700033.
- [73] Z.V. Borges, C.M. Poffo, J.C. De Lima, S.M. De Souza, D.M. Trichès, T.P.O. Nogueira, L. Manzato, R.S. De Biasi, Study of structural, optical and thermal properties of nanostructured SnSe<sub>2</sub> prepared by mechanical alloying, Mater. Chem. Phys. 169 (2016) 47–54.
- [74] J.F.G. Kresse, Efficient iterative schemes for ab initio total-energy calculations using a plane-wave basis set, Phys. Rev. B 54 (16) (1996) 11169–11186.
- [75] K.B. John, P. Perdew, Matthias Ernzerhof, Generalized gradient approximation made simple, Phys. Rev. Lett. 77 (18) (1996) 3865–3868.
- [76] D.J.G. Kresse, From ultrasoft pseudopotentials to the projector augmented-wave method, Phys. Rev. B 59 (3) (1999) 1758–1775.
- [77] P.E. Blöchl, Projector augmented-wave method, Phys. Rev. B 50 (1994) 17953–17979.
- [78] K. Mathew, J.H. Montoya, A. Faghaninia, S. Dwarakanath, M. Aykol, H. Tang, I.-h. Chu, T. Smidt, B. Bocklund, M. Horton, J. Dagdelen, B. Wood, Z.-K. Liu, J. Neaton, S.P. Ong, K. Persson, A. Jain, Atomate: a high-level interface to generate, execute, and analyze computational materials science workflows, Comp. Mater. Sci. 139 (2017) 140–152.
- [79] S. Grimme, Semiempirical GGA-type density functional constructed with a long-range dispersion correction, J. Comput. Chem. 27 (2006) 1787–1799.
- [80] M. De Jong, W. Chen, T. Angsten, A. Jain, R. Notestine, A. Gamst, M. Sluiter, C. Krishna Ande, S. Van Der Zwaag, J.J. Plata, C. Toher, S. Curtarolo, G. Ceder, K.A. Persson, M. Asta, Charting the complete elastic properties of inorganic crystalline compounds, Sci. data 2 (2015), 150009.
- [81] S.P.O. Anubhav Jain, Geoffroy Hautier, Charles Moore, <https://materialsproject.org/docs/calculations>.
- [82] G. Hautier, A. Miglio, D. Waroquiers, G.-M. Rignanese, X. Gonze, How does chemistry influence electron effective mass in Oxides? A high-throughput computational analysis, Chem. Mater. 26 (2014) 5447–5458.
- [83] G.K.H. Madsen, D.J. Singh, BoltzTraP: A code for calculating band-structure dependent quantities, Comput. Phys. Commun. 175 (2006) 67–71.
- [84] G. Ding, G.Y. Gao, Z. Huang, W. Zhang, K. Yao, Thermoelectric properties of monolayer MSe<sub>2</sub> (M = Zr, Hf): low lattice thermal conductivity and a promising figure of merit, Nanotechnology 27 (2016), 375703.
- [85] K.J. Koski, Y. Cui, The new skinny in two-dimensional nanomaterials, Acs Nano 7 (2013) 3739–3743.
- [86] F. Lotgering, Topotactical reactions with ferrimagnetic oxides having hexagonal crystal structures—I, J. Inorg. Nucl. Chem. 9 (1959) 113–123.
- [87] H.A. Lyden, Measurement of the conductivity effective mass in semiconductors using infrared reflection, Phys. Rev. 134 (1964) A1106–A1112.
- [88] D.G. Cahill, S.K. Watson, R.O. Pohl, Lower limit to the thermal conductivity of disordered crystals, Phys. Rev. B 46 (1992) 6131.
- [89] B. Qiu, L. Sun, X. Ruan, Lattice thermal conductivity reduction in Bi<sub>2</sub>Te<sub>3</sub> quantum wires with smooth and rough surfaces: a molecular dynamics study, Phys. Rev. B 83 (2011), 035312.